Engineered Science
DOI: https://dx.doi.org/10.30919/es8d852

Research on the Effect of Mean Stress and Dwell Position on The Fatigue Properties of Powder Superalloy (FGH95)

Zhifeng Yao,[1] Jundong Wang,[2,*] Tianyu Liu[2] and Chenyang Du[2]

Abstract

Fatigue tests were conducted on powder superalloy (FGH95) at a temperature of 650°C considering the effects of mean stress and stress dwell time. Standard specimens and two distinct geometric forms of notched specimens were utilized in the study. It is observed that the fatigue lives of the standard specimens followed a consistent S-shaped pattern with increasing the mean stress. In stress dwell tests, both types of notched specimens exhibited nearly identical fatigue lives for the maximum and minimum stress dwells (MAX-D, MIN-D). The experimental findings were analyzed using a damage-coupled unified creep-plasticity (D-UCP) constitutive model. For MAX-D, a notable accumulation of cumulative damage was observed within the initial cycles, with the rate of damage evolution rapidly saturating in subsequent cycles. Conversely, for MIN-D, although the cumulative damage in the initial cycles was relatively modest, the rate of damage evolution was significantly higher compared to the MAX-D condition. These factors collectively contribute to the gradual convergence of cumulative damage under both MAX-D and MIN-D conditions, providing an explanation for the approximately equal lifespan between the two loading conditions.

Keywords: Powder superalloy; Fatigue life; Mean stress; Notched specimen.
Received: 17 January 2024; Revised: 27 May 2024; Accepted: 14 June 2024.
Article type: Research article.

1. Introduction

Due to the advantages of uniform structure, fine grains, high temperature resistance and good fatigue resistance, powder superalloy have become a preferred material for the advanced aircraft engine components such as turbine discs. With the continuous development of the aviation industry, the working environment of aircraft engine components has become increasingly harsh. Turbine blades usually are subject to the fatigue-creep coupling effect with different mean stresses and different dwell times during operation, which usually leads to the catastrophic failure under complex damage modes. The existence of geometric features such as film holes, pin fins and vane trailing edge slots on the blades further weakens the structural strength due to the varying degrees of stress concentration.[1-3] Compared to the uniaxial stress state in laboratory conditions, the multi-axial stress state generated by these geometric discontinuities significantly affects the fatigue performance of powder superalloys. The high cycle fatigue (HCF) and low cycle fatigue (LCF) tests of nickel-based superalloy smooth specimens have been widely researched in the literature[4-10] while there is limited research on notched specimens. Therefore, it is crucial to research the fatigue performance of notched powder superalloys under different mean stress and stress concentration conditions at typical temperatures.

For nickel-based powder metallurgy, ambient temperature, load level, mean stress, and dwell time have a significant effect on fatigue life.[9-11] Bache *et al*.[12-13] performed a 100-hour oxidation treatment before MAX-D and MIN-D fatigue tests of powder superalloy notched specimens, and it was observed that the both environment and the stress dwell position can cause significant differences in fatigue life. The difference in fatigue life caused by MAX-D and MIN-D can be explained by the stress relaxation at the notch tip during fatigue loading. Similar conclusions were obtained from Telesman *et al*.,[14] and

[1] *School of Civil Engineering, Xi'an University of Architecture & Technology, Xi'an 710055, China.*
[2] *State Key Laboratory of Clean and Efficient Turbomachinery Power Equipment, School of Mechanics, Civil Engineering and Architextremely, Northwestern Polytechnical University, Xi'an, 710072, China.*
**Email:* wangjundong@nwpu.edu.cn (J. Wang)

the Drucker-Prager flow model was used to simulate the cyclic stress-strain behavior at the notch tip, which indicated the controlling role of stress triaxiality on the redistribution of the notch tip stress. The effect of dwell times on the LCF behaviour of nickel-based superalloy EI698 VD has also been investigated by Zrnik *et al*.,[15] and two regression functions for the applied dwell period interval were proposed to calculate the time to failure. Although some research on the effect of dwell time on fatigue life has been carried out in the aforementioned literature, further discussion is needed regarding the stress dwell position, such as dwell at minimum stress in the fatigue cycle.

Not only dwell time during fatigue cycle, but high mean stress will also cause complex fatigue-creep coupling damage. Kunz *et al*.[16-20] points out that different mean stress notably influences the HCF behaviors and fatigue failure mechanism of superalloy, but research on LCF remains insufficient. Cui *et al*.[21] conducted experimental and morphological analyses to investigate the influence of temperature on the LCF life of FGH95 alloy under different mean stress, and it was found that as a cyclic hardening material,[22] the fracture surfaces exhibited clear crack lines without patterns, which may not involve significant plastic deformation. It was considered that the LCF life of FGH95 was primarily determined by the crack initiation stage. Nonetheless, Cui's study had limited sample sizes for different mean stresses, so the conclusion of regularity could not be further summarized. Xu *et al*.[23] studied the effects of mean stress and temperature on short crack growth of FGH96 powder superalloy, and an engineering method of short crack growth life prediction based on Tanaka model[24] was proposed. However, the proposed model has not been fully validated due to the limited stress ratio conditions selected for the test.

In this study, fatigue tests of powder superalloy were conducted under different mean stress, *i.e.*, R=0, R=0.154, R=0.308, R=0.462, R=0.615, and R=0.769, as well as MAX-D/MIN-D with standard specimens and two different geometric forms of notched specimens at 650°C. In the second section, the experimental results were organized, revealing that under fatigue loading conditions, the cyclic life does not exhibit a linear relationship with mean stress, but rather demonstrates a fluctuating trend resembling an "S" shape. The number of crack initiation zones in the specimens shows a trend of initial increase followed by a decrease with mean stress. In the stress dwell test, similar numbers of cycles were observed for notched specimens under different holding position conditions, which deviated from the expected results. To further analyze the experimental results, the research of scholars such as Basaran *et al*.[25-33] on damage modeling was referenced. In the third section, the D-UCP model was established to provide simulated data for subsequent investigations. The fourth section discussed the influence of mean stress on fracture characteristics and fatigue life. By integrating experimental and simulated data, the results explained the similar number of cycles for notched specimens under different holding position conditions in the stress dwell test. Finally, the relationship between the fatigue life and the crack initiation stage was discussed.

2. Experimental procedure

2.1 Material and test conditions

The material employed in this study is a powder superalloy γ' phase precipitation-strengthened nickel-based alloy named as FGH95. It is primarily utilized in the disk components of aero-engine. The as-cast FGH95 undergoes a standard heat isostatic pressing (HIP) process, as well as solution treatment and aging procedures (solution treatment: 1140°C±10°C, 4 hours; salt bath 650°C±10°C 1 hour, followed by oil cooling; aging: 870°C±10°C, 1 hour, followed by air cooling 650°C±10°C, 24 hours). The main chemical composition of the FGH95 alloy is presented in Table 1.

Three types of specimens shown in Fig. 1 were used in experiments to study the influences of mean stress and MAX-D/MIN-D on the fatigue properties of FGH95. The smooth specimen (Fig. 1a) was used to study the effects of mean stress on the crack initiation and fatigue life of FGH95. All these smooth specimens were tested under a constant maximum stress with different mean stresses. Circular notched specimen (Fig. 1b) and V-notched specimen (Fig. 1c) were used to research the effects of MAX-D/MIN-D on fatigue life of FGH95. For comparison, smooth specimen was also utilized in this type of test. All experiments were conducted at 650°C. The specific experimental conditions for smooth and notched specimens were presented in Tables 2 and 3, respectively.

Before the experiment, a naming convention for the specimens was established. Each specimen was assigned a unique identifier which includes the following information:

$$X_1\text{-}X_2\text{-DT-DS-x} \quad (1)$$

Table 1. The main chemical composition of the FGH95 alloy.(expressed in mass percentage %).

C	Cr	Co	W	Mo	Al	Ti	Nb	B	Zr	Ni
0.04 ～ 0.09	12.00～ 14.00	7.00 ～ 9.00	3.30～ 3.70	3.30 ～ 3.70	3.30 ～ 3.70	2.30 ～ 2.70	3.30 ～ 3.70	0.006 ～ 0.015	0.03～ 0.05	Balance

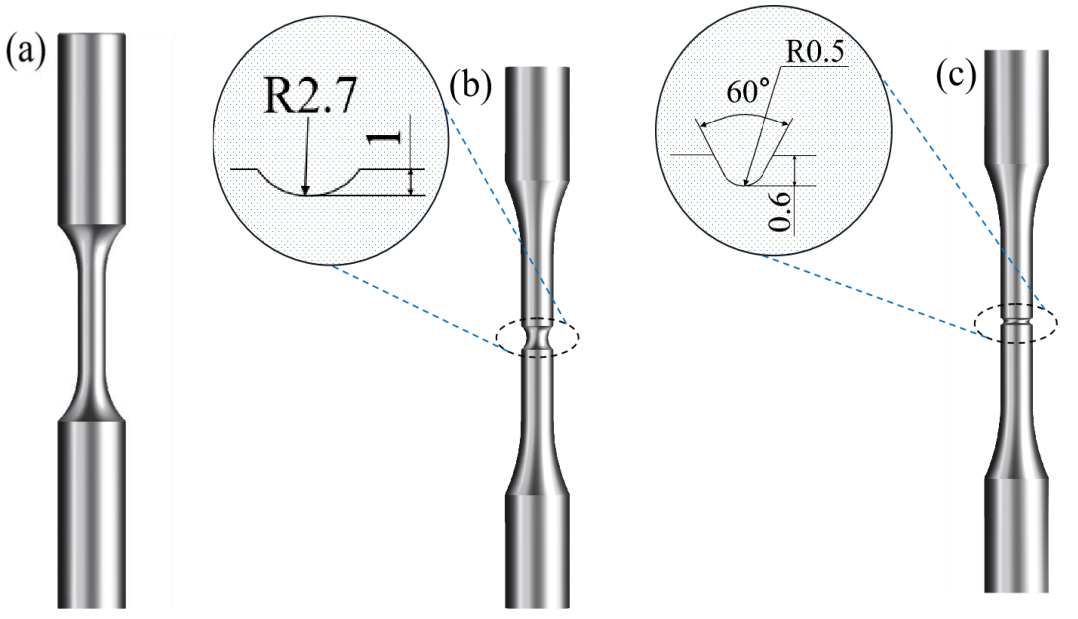

Fig. 1 The geometric of specimens used in this study ;(a) smooth specimen; (b) Circular notched specimen; (c) V-notch specimen.

Table 2. Test conditions of smooth specimens.

	Sample form	Mean stress (MPa)	Stress ratio	Identifier of specimen
Mean stress test	Smooth	650	0	S-0-0-0-1
		750	0.154	S-0.154-0-0-1
		850	0.308	S-0.308-0-0-1
		950	0.462	S-0.462-0-0-1
		1050	0.615	S-0.615-0-0-1
		1150	0.796	S-0.796-0-0-1

Table 3. Test conditions of notched specimens.

	Sample form	Maximum stress (MPa)	Dwell stress (MPa)	Identifier of specimen
Stress dwell test	Smooth	1300	1300	S-0.1-30-1300-1
				S-0.1-30-1300-2
			130	S-0.1-30-130-1
				S-0.1-30-130-2
		1350	1350	S-0.1-30-1350-1
			130	S-0.1-30-1350-2
	RCN	1300	1300	CN-0.1-30-1300-1
			130	CN-0.1-30-130-1
	VCN	1300	1300	VN-0.1-30-1300-1
			130	VN-0.1-30-130-1

where X_1 represents the geometric form of specimens. Here, S represents smooth specimen, CN and VN represent circular notched specimen and V-notch specimen, respectively. X_2 represents indicates the stress ratio of the test. DT represents the dwell time of test (unit second), DS indicates the dwell stress of test, x represents the number of the performed experiments.

All the tests were preformed at 650°C using a hydraulic-servo fatigue testing machine. The loading waveforms for different tests were shown in Fig. 2. The smooth specimens were subjected to fatigue cycles while maintaining a constant maximum stress of 1300MPa, but varying the mean stress level (see Fig. 2a). These tests were conducted at a frequency of 1Hz. For the MAX-D and MIN-D fatigue tests shown in Fig. 2b and Fig. 2c, three types of specimens were subjected to the loading with a 30 second dwell time at the maximum or minimum stress levels.

The fracture morphology of the sample, including the crack initiation zone, propagation zone, instantaneous fracture zone, cleavage steps, and ductile dimples, was examined using high-depth-of-field optical microscopy and scanning electron microscopy (SEM).

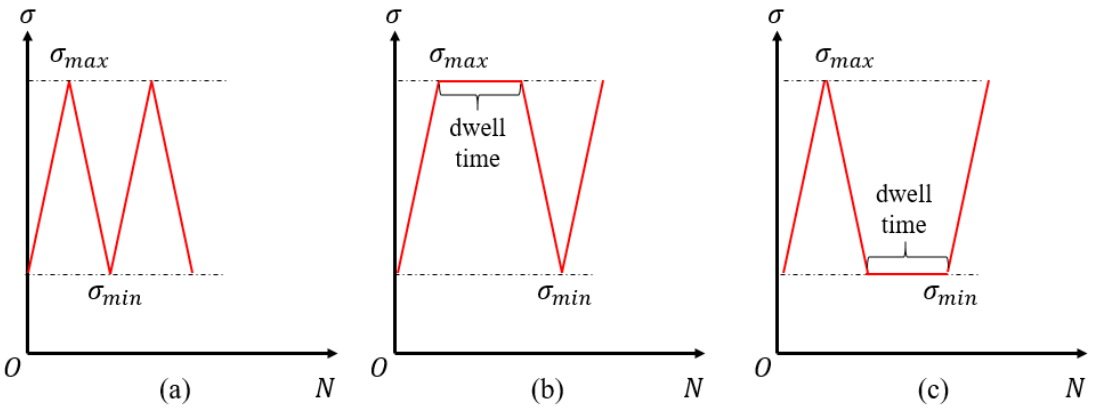

Fig. 2 Load spectrum for mean stress test and load protection test.

2.2 The fatigue test results of FGH95

The experimental results of different mean stress and different dwell positions were shown in Tables 4 and 5, repectively. As shown in Table 4, the fatigue life trend with different mean stresses, does not exhibit monotonic characteristics. As the mean stress increases, the fatigue life first decreases, then increases, and finally decreases again. This result is inconsistent with what was expected before the experiment. Detailed discussions on this matter will be provided in Section 3.2 of this paper.

Table 4. The experimental results of the mean stress test.

Identifier of specimen	Mean stress （MPa）	Fatigue life (cycles)	Number of crack initiation zone
S-0-0-0-1	650	1886	1
S-0.154-0-0-1	750	1425	6
S-0.308-0-0-1	850	1952	10
S-462-0-0-1	950	2230	12
S-0.615-0-0-1	1050	1128	1
S-0.796-0-0-1	1150	1768	1

The fatigue lives of different dwell time positions with smooth specimen, CN specimen and VN specimen were shown in Table 5. For smooth specimens, the dwell time on maximum stress significantly reduced fatigue life. In contrast, the results of CN specimens and VN specimens indicate that the fatigue life is not sensitive to dwell time position. Furthermore, the fatigue lives of CN and VN specimens tested under both MAX-D and MIN-D loading conditions are all longer than the fatgue lives of smooth specimens tested under the same loading conditions, which indicates the occurrence of notch strengthening during the dwell process.

2.3 The fatigue fracture characteristics of FGH95

Figure 3 presents the fracture surfaces of the smooth specimens obtained from different mean stress test. Fatigue cracks initiate at the surface of the specimens, appearing as light blue or light gray areas. The regions of crack initiation and instantaneous fracture exhibit distinct characteristics. Under high-depth-of-field microscopy, the crack initiation zones exhibit higher brightness, facilitating identification. The crack propagation zones appear as river-like patterns surrounding the initiation zones, while the remaining areas represent the instantaneous fracture region. Generally, the instantaneous fracture regions exhibit a 45-degree angle with respect to the stress axis. Additionally, the fracture surfaces display a certain degree of oxidation, resulting in darkening of the specimen's surface.

Table 5. Results of the stress dwell test.

Identifier of specimen	Fatigue life (cycles)	Number of crack initiation zone
S-0.1-30-1300-1	57	1
S-0.1-30-1300-2	127	1
S-0.1-30-130-1	1124	4
S-0.1-30-130-2	1625	30
S-0.1-30-1350-1	32	1
S-0.1-30-1350-2	1260	20
CN-0.1-30-1300-1	2470	1
CN-0.1-30-130-1	2476	1
VN-0.1-30-1300-1	250	1
VN-0.1-30-130-1	245	1

It was found that the number of crack initiation zones on the fracture surfaces of the specimens also shows the mean stress correlation. As the mean stress increases, the number of crack initiation zones first increases, and finally decreases. This is analogous to the trend observed in changes in fatigue life, as shown in the last column in Table 4.

The high-depth-of-field photo of fracture surfaces of MAX-D/MIN-D tests are shown in Figs. 4 and 5.

The characteristics of fracture surfaces in smooth specimens are reminiscent of those observed in mean stress

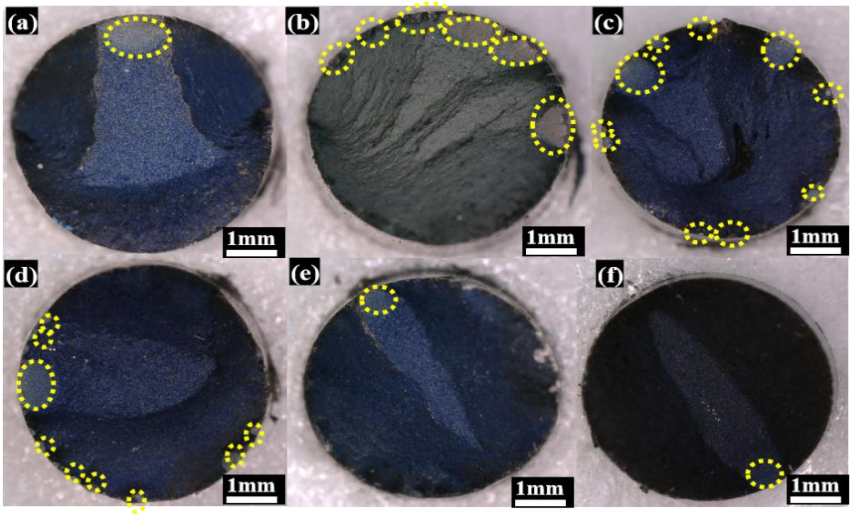

Fig. 3 High-depth-of-field photographs of fracture surfaces under various mean stress levels, N is the Number of crack initiation zone (a) 650MPa N=1; (b) 750MPa N=6; (c) 850MPa N=10; (d) 950MPa N=12; (e) 1050MPa N=1; (f) 1150MPa N=1.

tests. Both exhibit distinct bright crack initiation zones, river-like crack growth bands, and instantaneous fracture regions inclined at a 45° angle to the stress axis. The difference is that the crack initiation zones under dwell conditions display a yellow region enveloped by a pale blue region. Furthermore, under MAX-D conditions, the specimen has a single crack source, while under MIN-D conditions, the specimen has multiple crack sources. This result is consistent with the findings of Bache's research.[34] It is because under MIN-D conditions, the formation of surface breaking grain Boundaries promotes the early formation of cracks.

The notched specimen exhibits a larger crack initiation zone. In the CN specimen, the crack initiation zone accounts for approximately 6% of the fracture area, characterized by a yellow area surrounded by a light blue region, with the crack propagation zone relatively flat and the instantaneous fracture region exhibiting a cup-cone shape. The VN specimen features an annular crack initiation zone, with a flat and relatively large crack propagation zone, and the instantaneous fracture region inclined at a 45-degree angle to the stress axis.

Under MIN-D conditions, smooth specimens exhibit multiple crack initiation regions. Based on experimental findings, it is observed that specimens with a higher number of cycles also have a greater quantity of crack initiation zones. Therefore, it can be inferred that there exists a certain interaction between the number of cycles and the initiation zones of cracks. A detailed discussion on this matter will be provided in Section 4.4 of this study.

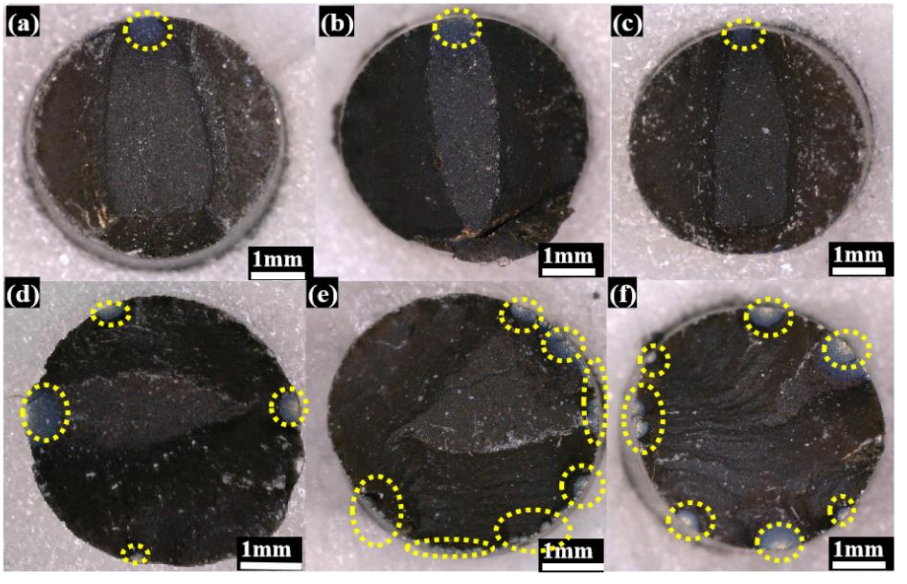

Fig. 4 High-depth-of-field photographs of fracture surfaces of smooth components under different stress levels during stress dwell conditions, N is the Number of crack initiation zone (a) 1300MPa N=1; (b) 1300MPa N=1; (c) 1350MPa N=1; (d) 130MPa N=4; (e) 130MPa N=30; (f) 135MPa N=20.

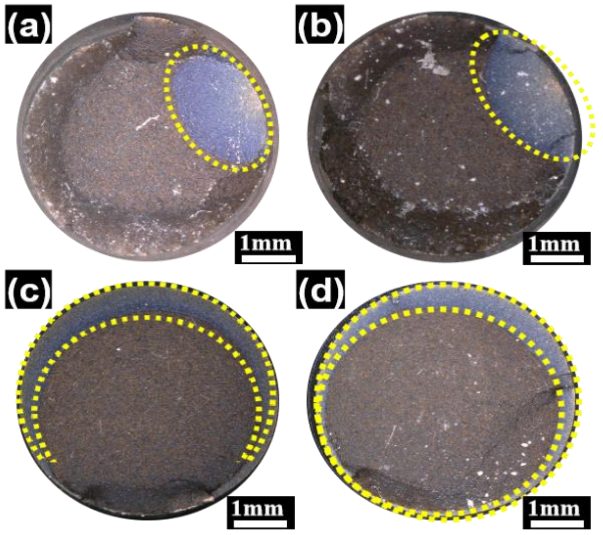

Fig. 5 High-depth-of-field photographs of fracture surfaces of notched components during stress dwell conditions N is the Number of crack initiation zone (a) Circular notched specimen under MAX-D conditions N=1; (b) Circular notched specimen under MIN-D N=1; (c) V-notch specimen under MAX-D conditions N=1; (d) V-notch specimen under MIN-D N=1.

3 Theoretical model

3.1 Constitutive model based on the unified creep plasticity theory

To further analyze the different fatigue behavior under different mean stresses and MAX-D/MIN-D a damage-coupled unified creep-plasticity (D-UCP) constitutive model was employed. In this D-UCP theory, the plastic strain and creep strain are combined into a non-elastic strain, and the total strain can be expressed in the following form:

$$\dot{\boldsymbol{\varepsilon}} = \dot{\boldsymbol{\varepsilon}}^{e} + \dot{\boldsymbol{\varepsilon}}^{in} + \dot{\boldsymbol{\varepsilon}}^{T} \tag{2}$$

where $\dot{\varepsilon}^{in}$ is the rate of non-elastic strain. The calculation formula for the rate of non-elastic strain is the main distinguishing feature of the UCP model. The following McDowell[35-36] model coupled with a strain-based damage model was adopted to analyze the stress-strain distribution of the notched specimens:

$$\dot{\boldsymbol{\varepsilon}}^{in} = A\left(\frac{S_v}{d}\right)^{n} exp\left[B\left(\frac{S_v}{d}\right)^{n+1}\right] exp\left(-\frac{Q}{\theta T}\right)\boldsymbol{N} \tag{3}$$

$$S_v = \left\langle \sqrt{\frac{3}{2}}\frac{1}{1-D}\|\boldsymbol{S}-\boldsymbol{\alpha}\| - R \right\rangle \tag{4}$$

$$\boldsymbol{N} = \frac{\boldsymbol{S}-\boldsymbol{\alpha}}{\|\boldsymbol{S}-\boldsymbol{\alpha}\|} \tag{5}$$

where θ is the gas constant, $\boldsymbol{\alpha}$ is the back stress tensor, d is the reference stress, R is the instantaneous yield surface radius, D is the damage factors. When D equals 0, it indicates no damage in material, while D equals 1 indicates complete loss of load-bearing capacity in material. In practice, materials often lose their serviceability before D reaches 1, so a critical damage value, D_{cr}, is established as a value less than 1. When the damage value exceeds D_{cr}, the material is considered to be completely destroyed. The Macaulay bracket $\langle\rangle$ (when $H \geq 0$, $\langle H\rangle = H$; when $H < 0$, $\langle H\rangle = 0$). $\boldsymbol{S}$ is the deviatoric stress tensor:

$$\boldsymbol{S} = \boldsymbol{\sigma} - \frac{1}{3}tr(\boldsymbol{\sigma}) \tag{6}$$

In the case of small deformation, the change of stress rate tensor can be obtained as follows:

$$\dot{\boldsymbol{\sigma}} = (1-D)C(T):\left(\dot{\varepsilon} - \dot{\varepsilon}^{in} - \dot{\varepsilon}^{T}\right) \tag{7}$$

$\boldsymbol{\sigma}$ represents the Cauchy stress tensor, $C(T)$ signifies the temperature dependent elastic modulus. During the initial loading stage, the material strength gradually increases due to strain hardening, leading to an expansion of the yield surface radius. As the loading continues, the rate of hardening typically diminishes, resulting in a slower growth of the yield surface radius. Therefore, the evolution of the yield radius is defined as follows:

$$R = R_0 + (R_\infty - R_0)\left(1 - e^{-b\varepsilon_{eq}^{in}}\right) \tag{8}$$

R_0 is the initial yield stress, which can be determined through the material's initial yielding behavior. R_∞ is the saturation value. The material constant b which controls the rate at which the saturation value is achieved, ε_{eq}^{in} is the cumulative plastic strain:

$$\varepsilon_{eq}^{in} = \sqrt{\int_0^t \frac{2}{3}\varepsilon_{ij}^{in}\varepsilon_{ij}^{in}dt} \tag{9}$$

During cyclic loading of metallic materials, strain hardening not only causes the equivalently expand of yield surface, but also induces the center of the yield surface translation in stress space.[37-39] The the latter is characterized by a constant yield radius, while the center position of the yield surface moves with the variation of back stresses, which is referred to as kinematic hardening. In this study, the Prager model[40-42] is employed to calculate the back stresses:

$$\dot{\boldsymbol{\alpha}} = \mu\left\|\dot{\boldsymbol{\varepsilon}}^{in}\right\|\boldsymbol{N} - \beta\boldsymbol{\alpha} \tag{10}$$

In the above equation, μ and β are both material constants. Similar to the yield stress, the back stress calculated by equation (10) will eventually reach a saturation value and no longer increase. The $\left\|\dot{\boldsymbol{\varepsilon}}^{\boldsymbol{in}}\right\|$ in Eq. (10) is defined as:

$$\left\|\dot{\boldsymbol{\varepsilon}}^{in}\right\| = \sqrt{\frac{2}{3}\dot{\varepsilon}_{ij}^{in}\dot{\varepsilon}_{ij}^{in}} \tag{11}$$

In order to study the effects of different mean stress and MAX-D/MIN-D on fatigue life, the following strain-based damage evolution model[43-45] was used:

$$f\left(\frac{\sigma_H}{\sigma_{eq}}\right) = \frac{2}{3}(1+v) + 3(1-2v)\left(\frac{\sigma_H}{\sigma_{eq}}\right)^2 \tag{12}$$

$$\mathrm{d}D = \alpha\frac{(D_{cr}-D_0)^{1/\alpha}}{\ln(\varepsilon_{cr}/\varepsilon_{th})} f\left(\frac{\sigma_H}{\sigma_{eq}}\right)(D_{cr}-D)^{(\alpha-1)/\alpha}\frac{\mathrm{d}p}{p} \tag{13}$$

where ε_{th} is the threshold strain corresponding to D_0, ε_{cr} is the strain at failure corresponding to D_{cr}, $\boldsymbol{\alpha}$ is the damage exponent which controls the process of damage evolution, v is poisson's ratio, σ_{eq} is the equivalent von Mises stress, σ_H is the hydrostatic stress, p is the accumulated inelastic strain. By incorporating the above fatigue damage evolution equation into the UCP constitutive model, the influence of mean stress and MAX-D/MIN-D on damage accumulation process during fatigue loading can be considered.

3.2 Constitutive model parameters

To apply the aforementioned damage coupled constitutive model in fatigue damage assessment, it is essential to obtain the constitutive model parameters at the corresponding temperature. The mechanical properties of FGH95 alloy and the constitutive parameters used in the simulation are presented in Tables 6 and 7, respectively.

Table 6. Properties of FGH95 alloy tested at 650 ℃.

Loading condition	Tensile strength σ_b/MPa	Yield strength $\sigma_{0.2}$/MPa	Elongation δ_5/%	Reduction of area Ψ/%
650 ℃	1506	1190	13.4	16.8

Table 7. Constitutive parameters.

Symbol	Physical meaning	Value
D_0	Initial value of damage	0
D_{cr}	Critical value of damage at failure	1
ε_{cr}	Strain at failure corresponding to D_{cr}	0.3
ε_{th}	Threshold strain corresponding to D_0	0.005
E	Elastic modulus	177GPa
v	Poisson's ratio	0.333
α	Damage exponent of the material	0.09

The finite element models for the three types of specimens were established in Abaqus software. The smooth specimens were constructed in a three-dimensional model space using a single cubic element for computation. As for the notched specimens, an axisymmetric model space was employed, with grid refinement at the notch using approximately 500 quadrilateral meshes. Isotropic hardening parameters (R_0 and R_∞) were determined using the yield behaviour of the considered FGH95 alloy which was obtained from uniaxial tensile test data. Additionally, the kinematic hardening parameters (μandβ) were determined based on the stress-strain behavior of the smooth specimen that was tested under stress-controlled fatigue cycle loadings.

Based on the D-UCP model, a three-dimensional finite element analysis was conducted. Uniaxial cyclic fatigue loading was applied to the smooth round bar model under the same loading conditions as the specimen S-0-0-0-1, *i.e.*, maximum stress of 1300MPa, stress ratio R=0, and temperature of 650°C. The stress-strain curves from the experiments and simulations are shown in Fig. 6. The simulation results agree well with the experimental data, indicating that the D-UCP model can simulate the mechanical properties of FGH95 alloy under these loading conditions. This demonstrates the accuracy and applicability of the model in predicting the constitutive behavior of FGH95 alloy materials.

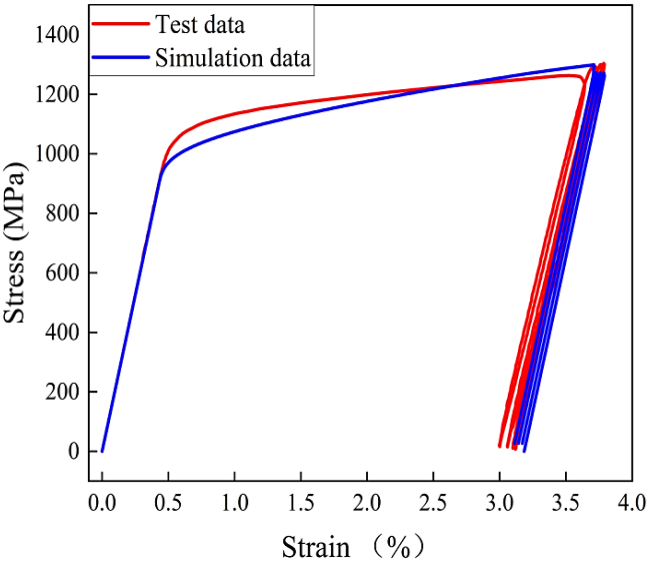

Fig. 6 Comparison between experimental and simulated hysteretic curve.

4. Results and discussion

4.1 The Effect of mean stress on the fracture characteristics

The experimental results in Section 2.2 demonstrate that, at a maximum stress of 1300MPa, the fatigue life of powder superalloy does not exhibit a linear relationship with the mean stress but rather displays a fluctuating trend resembling an S shape as the mean stress increases. This experimental result indicates the existence of a certain degree of interaction between stress amplitude (fatigue component) and mean stress (creep component). This coupling effect of fatigue and creep to some extent affects the number of cycles of the specimen.

Figure 7 depicts the evolution of cumulative plastic strain (ratchet strain) and the cumulative plastic strain at the point of fracture obtained through experimental measurements under varying average stress levels. While the cyclic life of the specimen does not exhibit a linear relationship with the mean stress, the accumulated plastic strain of the specimen demonstrates a monotonic variation with increasing mean stress.

In Fig. 7(a), it can be observed that as the mean stress

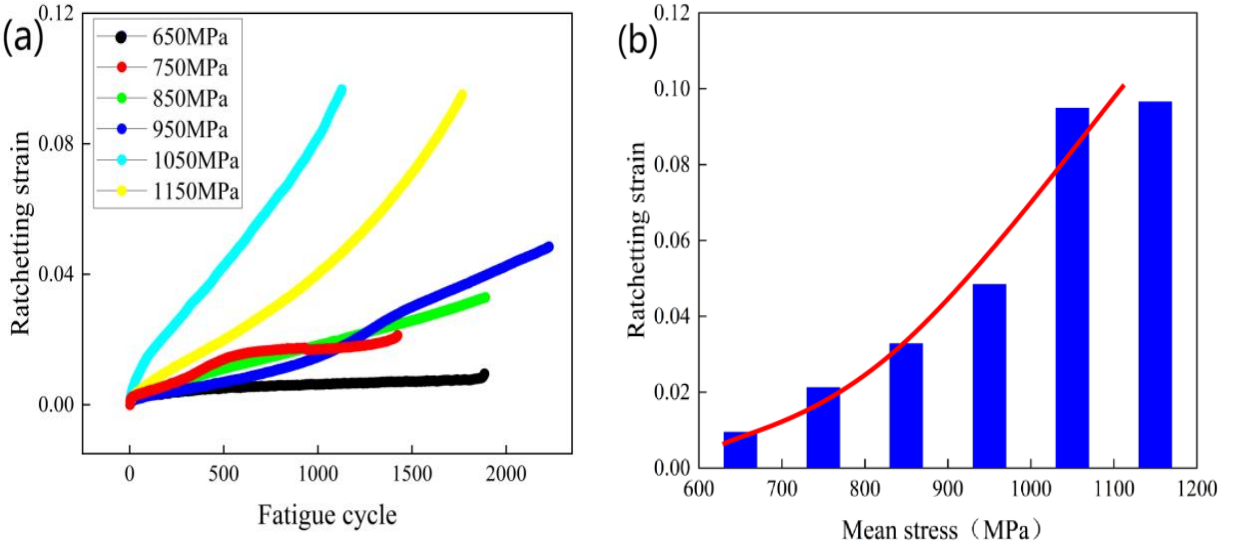

Fig. 7 (a) Evolution of cumulative plastic strain under different mean stress levels; (b) Cumulative plastic strain at fracture.

increases, the slope of the curves depicting plastic strain evolution for 650MPa and 750MPa follows a logarithmic form, which is a typical mode of plastic strain evolution in fatigue cyclic tests. The curves for 850MPa and 950MPa demonstrate an approximately linear distribution at an angle of 20°, suggesting the interaction between fatigue and creep components. The plastic strain evolution curves for 1050MPa and 1150MPa exhibit an exponential form with a significant increase in slope, representing a typical mode of plastic strain evolution in creep tests.

By combining the observations from Fig. 7(a) and Fig. 7(b), it can be reasonably inferred that, in mean stress tests, as the mean stress increases, the creep component also increases, leading to a transition from fatigue failure to creep failure in the fracture behavior of the specimens. To validate this hypothesis, scanning electron microscopy analysis was performed on the microstructure of fracture surfaces.

Figure 8 presents the micro structural features of fracture surfaces under different mean stresses. The microstructure reveals that at the mean stress of 650MPa, distinct small fracture planes are observed, with minimal evidence of dimples, indicating that the failure of the specimens is primarily attributed to fatigue. At the mean stresses of 750MPa, 850MPa, and 950MPa, both cleavage steps and dimple morphological are observed on the fracture surfaces, indicating a combined effect of fatigue and creep in the fracture mechanism.[46] Conversely, at the mean stresses of 1050MPa and 1150MPa, the fracture surfaces exhibit minimal presence of cleavage steps or brittle fracture features, providing evidence that the failure of the specimens is

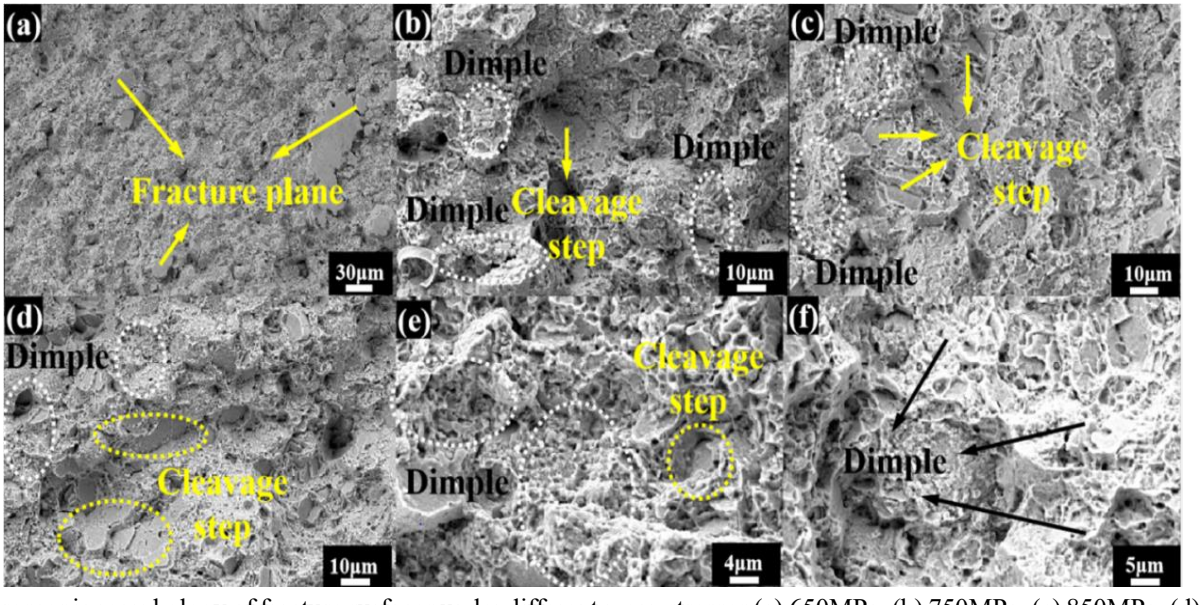

Fig. 8 Microscopic morphology of fracture surfaces under different mean stresses (a) 650MPa; (b) 750MPa; (c) 850MPa; (d) 950MPa; (e) 1050MPa; (f) 1150MPa.

predominantly caused by creep behavior. These findings effectively substantiate the hypothesis regarding the influence of mean stress on the fracture mode as discussed earlier.

4.2 The effect of mean stress on fatigue life

In Section 4.1, it was shown that the failure of specimens stemmed from the interaction between the two components of fatigue and creep. Li[47] considers that these two components mainly manifest as the mean stress (the creep component) and the cyclic stress amplitude (the fatigue component), which have an influence on the initiation and propagation of cracks. The mean stress controls the crack initiation process of the alloy, and an increase in the mean stress will enhance the probability of crack initiation. On the contrary, an increase in the cyclic stress amplitude (the fatigue component) can promote the propagation of cracks that have already initiated. Therefore, an appropriate combination of mean stress and cyclic stress amplitude will generate a strong fatigue-creep interaction that significantly affects the material's cyclic life.

Figures. 9 and 10 illustrate the mean stress-life curve and the number of crack initiation sites as a function of mean stress for smooth round bar specimens. Fig. 9 illustrates an "S"-shaped relationship between the cyclic life and mean stress, which is similar to the experimental results obtained from the mean stress tests in Li's study (Fig. 9b). As the mean stress increased, the number of crack initiation sources in the fracture origin area showed a trend of first increasing and then decreasing. When the mean stress was 950MPa, the number of crack initiation sources reached a maximum of 12. When the mean stress is 950MPa, there is a common inflection point observed in both the cyclic stress curve and the curve depicting the number of crack initiation points. Specifically, when the mean stress is 750MPa, the fatigue life increases along with the increase of the number of crack initiation sites. And when the mean stress is 1050 MPa, the fatigue life decreases as the number of crack initiation sites decreases.

In summary, the influence of the changing mean stress and cyclic stress amplitude on the number of crack initiation sites can reasonably explain the experimental results regarding the specimen's fatigue life:

A lower mean stress reduces the probability of crack initiation and thereby extends prolongs the material's cyclic life. As the mean stress increases, the probability of crack initiation and the number of crack initiation sources also increase. However, simultaneously, the stress amplitude decreases, bring about a reduction in the crack propagation rate and an increase in the fatigue life. When the mean stress further increases, the crack initiation rate reaches a high level, resulting in the rapid appearance of the first crack initiation site, followed by crack propagation and specimen fracture, significantly reducing the fatigue life. When the mean stress reaches 1150MPa, corresponding to a stress ratio of approximately 0.88, the microscopic morphology in Fig. 8 exhibits characteristics of a creep fracture, such as a dense dimples structure with almost no brittle fracture steps. Therefore, the failure mode of the specimen can be approximated as pure creep behavior. The low stress amplitude prevents rapid crack propagation, resulting in a longer fatigue life compared to the 1050MPa fatigue test.

4.3 The Influence of dwell-time position on fatigue life

The results of cyclic creep-loading tests conducted on three different types of specimens were illustrated in Table 5.

The test results indicate that the cyclic fatigue life of smooth specimen under MIN-D conditions is significantly greater than that under MAX-D conditions. This is attributed to the presence of higher mean stress under MAX-D conditions, which makes the specimen more susceptible to failure. This finding aligns with the expectations of most scholars and will not be discussed in further detail here.

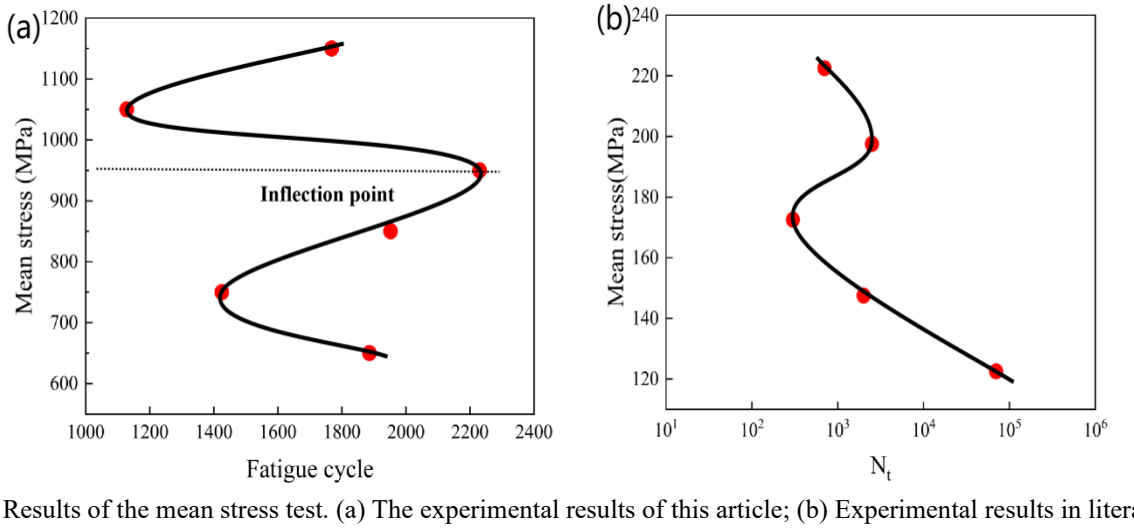

Fig. 9 Results of the mean stress test. (a) The experimental results of this article; (b) Experimental results in literature.

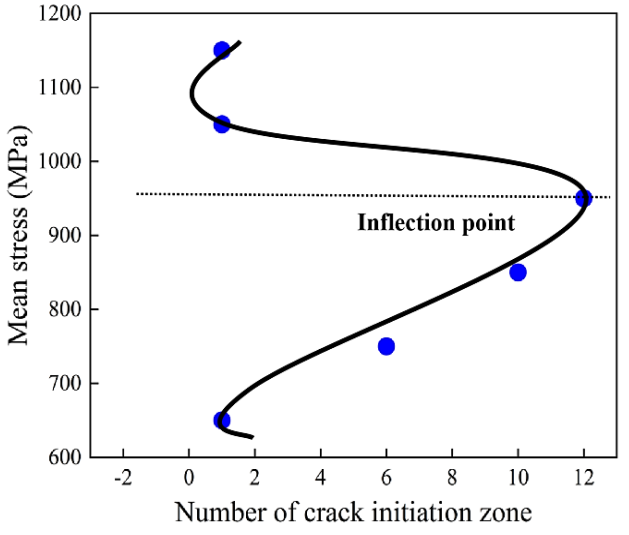

Fig. 10 Number of crack initiation zones on smooth cylindrical specimens at 650°C.

However, for notched specimens, there is essentially no difference in cyclic fatigue life under different stress dwell conditions. This may be related to the stress state at the notch. According to Bonora *et al*.,[48-51] the complex stress state has significant impact on damage mode.

Employing the theoretical model explicated in Chapter 3, finite element simulations were executed using Abaqus software. These simulations yielded results concerning the accumulation of damage, stress relaxation, and stress distribution at the notch root, as illustrated in Figs. 11, 12, 14, and 15.

Figure 11 illustrates the cumulative damage of different specimen types under simulated stress dwell conditions. Unlike the notched specimens, the cumulative damage of smooth specimens under MAX-D conditions exhibits a monotonically increasing exponential trend. The difference in cumulative damage between the MAX-D condition and the MIN-D condition rapidly increases with the number of cycles, resulting in a significantly higher failure rate for smooth specimens under MAX-D conditions compared to MIN-D conditions. This phenomenon provides an explanation for the experimental observation that the cycle period for failure is much greater for smooth specimens under MAX-D conditions than under MIN-D conditions.

The cumulative damage trends of CN and VN notched specimens under stress dwell conditions are largely similar. Under MAX-D conditions, the damage rapidly accumulates in the first 2-3 cycles before stabilizing, and after the 5th-6th cycle, the rate of cumulative damage decreases dramatically, reaching a very low level. Meanwhile, under MIN-D conditions, the damage continues to accumulate at a relatively

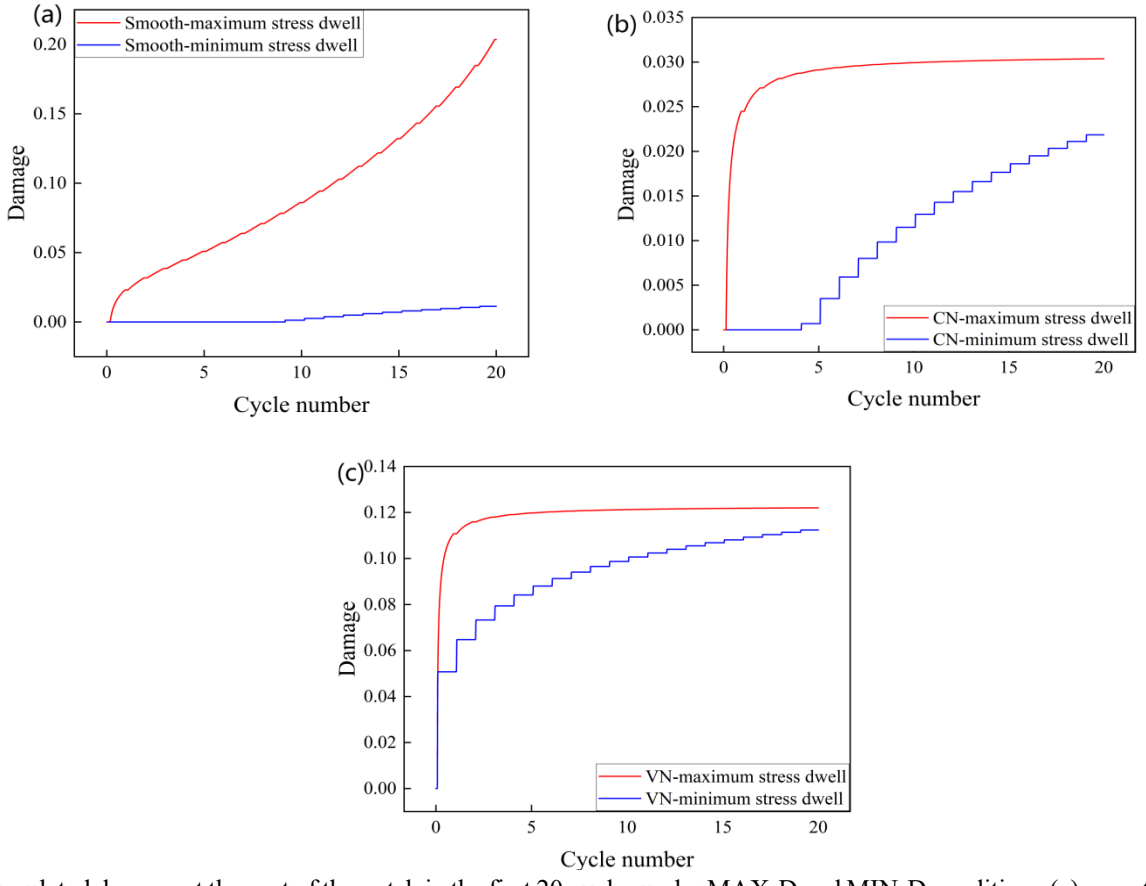

Fig. 11 Accumulated damage at the root of the notch in the first 20 cycles under MAX-D and MIN-D conditions.(a) smooth specimen; (b) Circular notched specimen; (c) V-notch specimen.

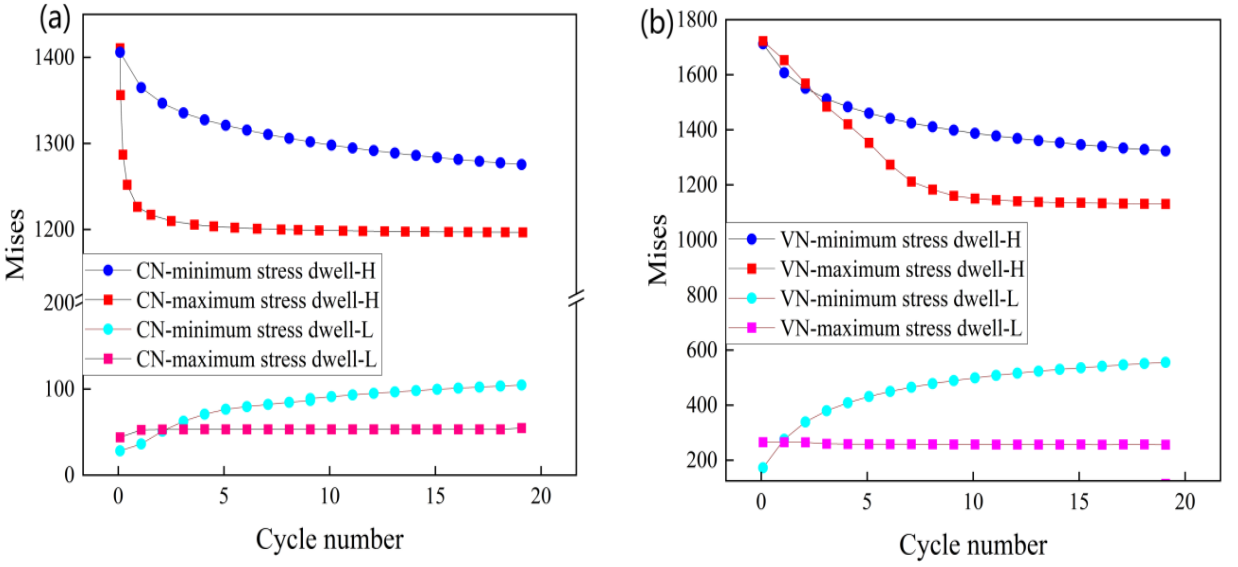

Fig. 12 Stress relaxation situation at the root of the notch in the first 20 cycles at peak (H) and valley (L) load values under MAX-D and MIN-D conditions. (a) Circular notched specimen; (b) V-notch specimen.

high speed at this point. As a result, with an increasing number of cycles, the cumulative damage under the two stress dwell conditions becomes increasingly similar, leading to comparable fatigue life. To further elucidate this phenomenon, this study simulated the stress relaxation at the notch root of the two notched specimens under stress dwell conditions.

Figure 12 illustrates the simulated stress relaxation at the notch root of two notched specimens under stress dwell conditions at the peak and valley of loading. It can be observed from this figure that the stress relaxation behavior of the two notched specimens is approximately similar.

At the peak of loading, compared to the MIN-D, the MAX-D exhibits a more pronounced stress relaxation. This is attributed to the rapid accumulation of plastic strain at the notch root under MAX-D conditions, as depicted in Fig. 13, leading to more noticeable stress relaxation. On the other hand, the slower rate of plastic strain accumulation under MIN-D conditions results in a slower stress relaxation at the notch root, thus maintaining relatively high Mises stress at the notch root at the peak of loading throughout the entire loading cycle.

On the other hand, at the valley of the loading cycle, the MIN-D exhibits a noticeable tendency of stress relaxation compared to the MAX-D. This phenomenon can be explained by the stress relaxation at the root of the notch as simulated. As shown in Fig. 14, under the MAX-D condition, the principal stress rapidly relaxes and then tends to stabilize, resulting in a relatively stable trend in von-Mises stress. Under the MIN-D condition, due to the slower accumulation rate of plastic strain, there is still a significant stress relaxation phenomenon in the third principal stress at the load valley. This leads to a continuous increase in the difference between the first and second principal stresses and the third principal

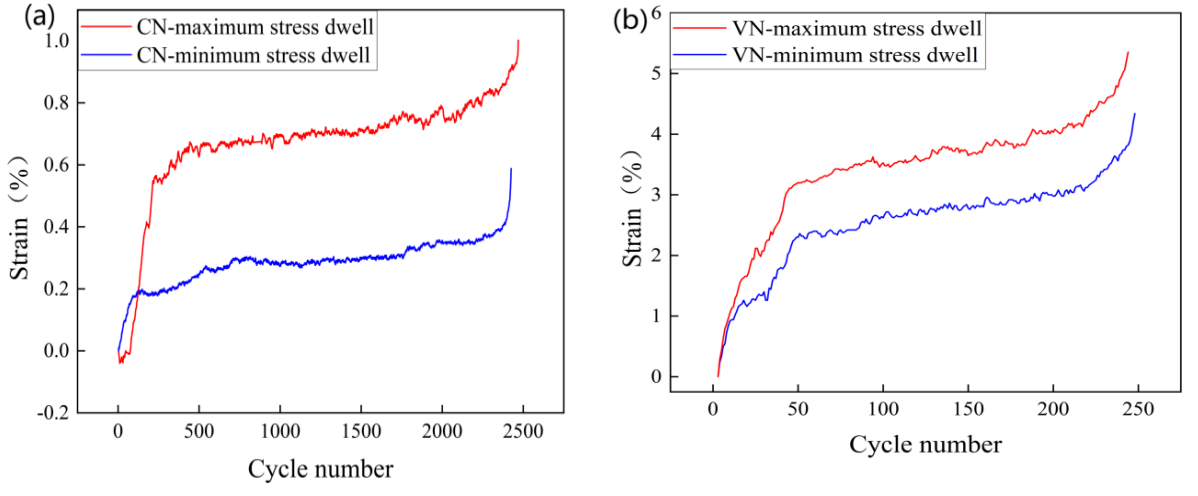

Fig. 13 Experimental data of accumulated plastic strain under stress dwell conditions. (a) Circular notched specimen; (b) V-notch specimen.

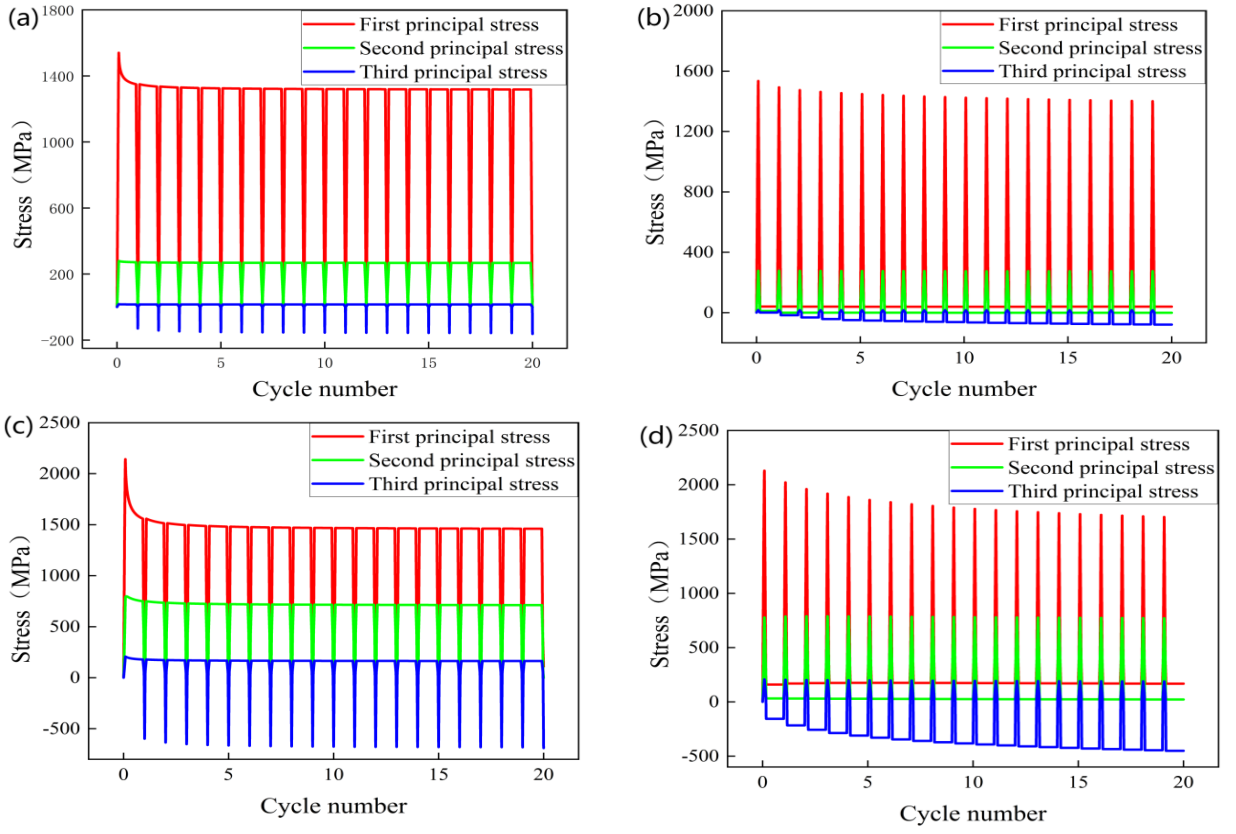

Fig. 14 Simulation results of the principal stress in notched specimens under stress dwell conditions. (a) Circular notched specimen under MAX-D conditions; (b) Circular notched specimen under MIN-D; (c) V-notch specimen under MAX-D conditions; (d) V-notch specimen under MIN-D.

stress, consequently causing the observed phenomenon of upward stress relaxation in the von-Mises stress, as depicted in Fig. 12. To sum up, throughout most cycles of the entire failure process, MIN-D exhibits higher von-Mises stress compared to MAX-D, regardless of whether it is at the peak or valley of loading. This leads to a steady accumulation of damage during the entire failure process under MIN-D conditions. This factor contribute to the gradual convergence of cumulative damage under both loading conditions, providing an explanation for the similarity in cycle counts between the two loading conditions.

As shown in Fig. 5, the crack initiation zone of the notched specimens under stress dwell conditions primarily occurs at the root of the notch. Hence, the magnitude of stress at the notch root can effectively influence the failure rate of the specimens.

By performing simulation calculations and normalizing the stress distribution at the center of the notch for the initial and twentieth cycles, Fig. 15 is obtained. It can be observed that the stress distribution in the VN specimen is mainly concentrated at the notch root, and in most cases, the stress at the notch root of the VN specimen surpasses that of the CN specimen. The reason for the occurrence of higher stress at the notch root of the CN specimen in Fig. 15(b) is that by the twentieth cycle, the VN specimen has already undergone significant plastic deformation and cumulative damage under MAX-D conditions, leading to evident stress relaxation. However, the stress distribution still predominantly concentrates at the notch root. Consequently, compared to the CN specimen, the VN specimen exhibits greater and more localized stress at the notch root. Moreover, Fig. 11 also demonstrates that the VN specimen accumulates more significant cumulative damage at the same number of cycles. The above analysis is summarized as follows. The cyclic fatigue life of the VN specimen is evidently lower than that of the CN specimen, which aligns with the obtained results (the cyclic fatigue life of the CN specimen is approximately ten times that of the VN specimen).

4.4 The relationship between cyclic life and crack initiation

The observation of fracture surfaces reveals a close relationship between the number of initiation sites in smooth specimens and their fatigue life, whereas this phenomenon is less pronounced in notched specimens. This can be attributed to the stress concentration at the root of notches, which hinders the occurrence of multiple crack initiation sites at the fracture

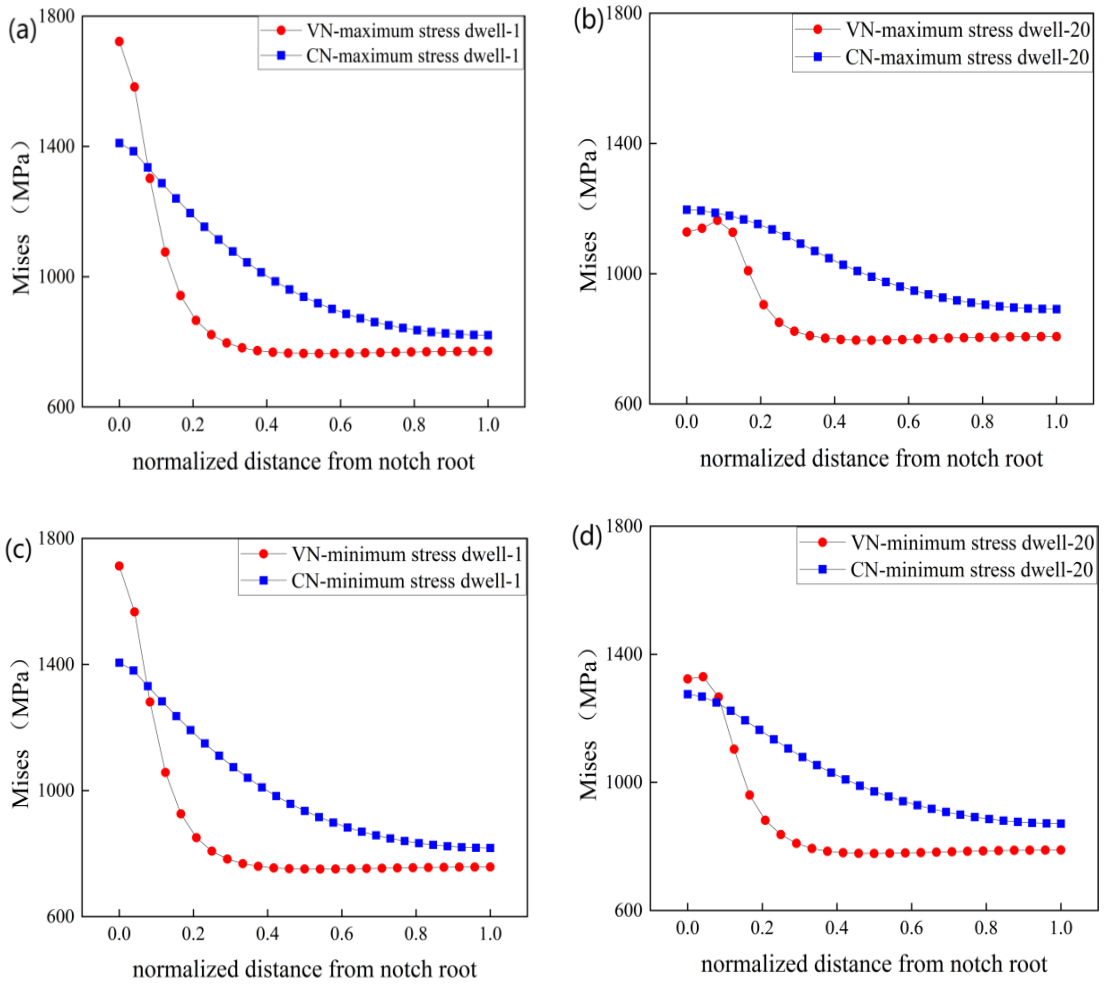

Fig. 15 Stress distribution along the notch root to the sample center. (a) The initial cycle under MAX-D condition; (b) The twentieth cycle under MAX-D condition.; (c) The initial cycle under MIN-D condition; (d) The twentieth cycle under MIN-D condition.

surface.

This section primarily focuses on the analysis and discussion of the relationship between the number of initiation sites and fatigue life in smooth specimens. Four plausible relationships can be inferred:

(1) Multiple initiation sites accelerate specimen failure and decrease fatigue life.

(2) Multiple initiation sites inhibit specimen failure and increase fatigue life.

(3) The number of initiation sites has no significant effect on specimen failure. However, appropriate loading conditions result in higher fatigue life, providing more time for the initiation of crack sources. This ultimately leads to the phenomenon observed in our experimental results, where specimens with longer fatigue life tend to have more crack initiation sites.

(4) Under the same loading conditions, a greater fatigue life will induce the initiation of more crack sources, while simultaneously multiple initiation sites will inhibit specimen failure and increase fatigue life. The entire failure process is characterized by the interaction between the number of initiation sites and the number of loading cycles.

From Fig. 17, it can be observed that the trend of crack initiation site numbers under their respective loading conditions is generally to increase with increasing fatigue life. In addition, the microgram images of smooth specimen fractures (Figs. 16 and 17) reveal that the relatively smaller crack sources in fractures with multiple initiation sites hardly extend into crack propagation areas. Instead, they are adjacent to the instantaneous fracture zone of the main crack initiation site. This suggests that the initiation and propagation of the main crack source are the primary causes of specimen fracture.Therefore, it can be inferred that the possibility that multiple initiation sites accelerate specimen failure and decrease fatigue life (hypothesis 1) can be largely ruled out.

In the discussion regarding hypotheses (2), (3), and (4), this study considers hypothesis (4) to be more reasonable. Specifically, under the same loading conditions, a larger fatigue life will lead to a greater number of crack initiation sites, while multiple initiation sites simultaneously inhibit

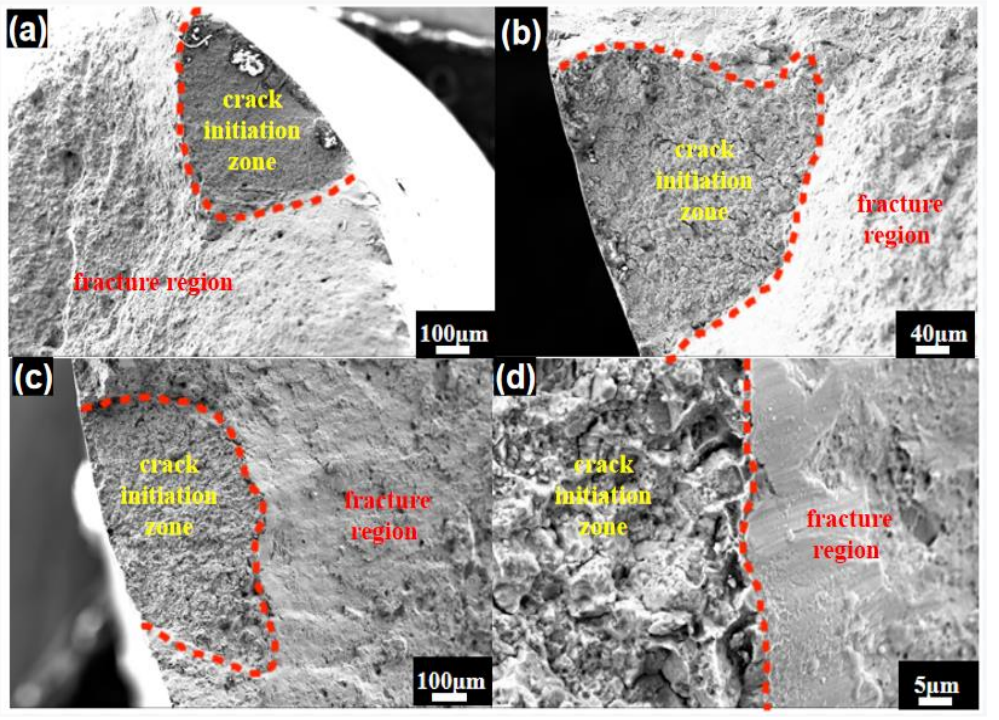

Fig. 16 Microscopic morphology of multiple crack initiation regions at fracture surfaces. (a) mean stress of 750MPa; (b) mean stress of 850MPa; (c) mean stress of 950MPa; (d) mean stress of 1050MPa.

specimen failure, thereby increasing the fatigue life. The entire failure process involves an interaction between the number of crack initiation sites and the number of cycles.

The conclusion that under the same loading conditions, a larger fatigue life will lead to a greater number of crack initiation sites requires minimal further debate. The mean stress controls the initiation of cracks in the alloy, as an increase in mean stress increases the probability of crack initiation. Furthermore, an increase in cyclic stress amplitude promotes the propagation of already initiated cracks. Under the same loading conditions, specimens with a longer fatigue life experience a greater duration of stress and a larger number of cyclic loading cycles, making crack initiation more likely. This relationship is illustrated by Fig. 18, which depicts the relationship between the number of crack initiation sites and fatigue life in the stress dwell test.

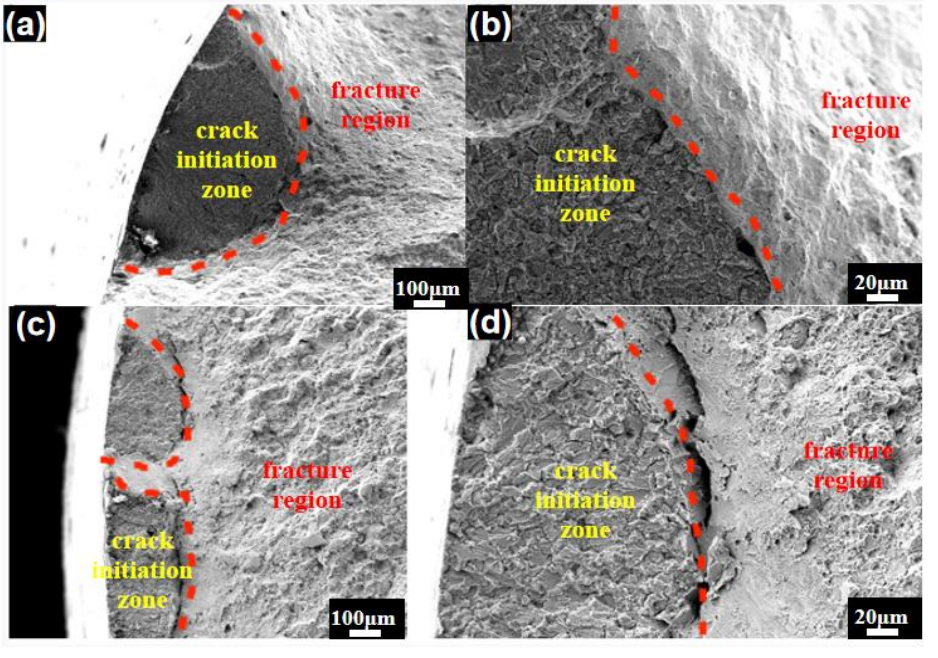

Fig. 17 Microscopic morphology of multiple crack initiation regions at fracture surfaces under different sustained stress levels. (a) Sustained stress of 135MPa; (b) Sustained stress of 135MPa; (c) Sustained stress of 130MPa; (d) Sustained stress of 130MPa.

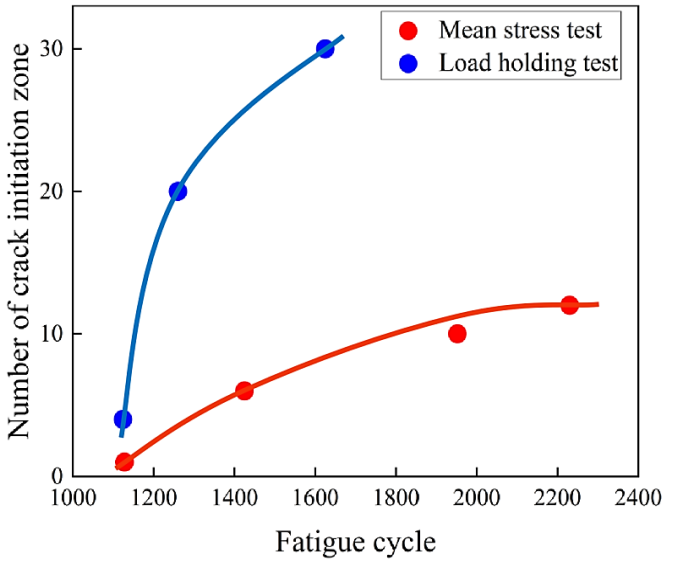

Fig. 18 The relationship between the quantity of crack initiation zones and the fatigue life in mean stress tests and MIN-D tests.

If assume that the relationship between the number of initiation sites and fatigue life is solely influenced by fatigue life, then the curve representing the relationship between the number of initiation sites and fatigue life within an appropriate loading range should be approximately linear. However, by observing Fig. 18, it becomes evident that both the valley load curve in the constant amplitude test under the same loading conditions and the mean stress test curve under different loading conditions follow a clear logarithmic function form. This suggests that a certain factor, which increases with fatigue life during the loading process, inhibits specimen failure and extends the fatigue life. Considering Fig. 10 as well, this study reasonably speculates that this factor is the increasing number of crack initiation sites associated with increasing fatigue life.

In the field of composite materials research, the phenomenon of crack toughening crack toughening phenomenon is widely recognized. The presence of cracks and impurities in a specimen can partially suppress the occurrence of failure to some extent. Literature indicates that cracks typically initiate from impurities during fatigue tests. Due to the heterogeneity between impurities and matrix materials, a mismatch strain occurs at the crack tip under the effect of singular stress fields, commonly referred to as phase transformation strain. The generation of phase transformation strain changes the system's energy, resulting in interaction forces (*i.e.*, configuration forces) between impurities and cracks. When hard impurities are present within the crack body (*i.e.*, impurities with a higher elastic modulus than the matrix materials), repulsive forces between impurities and cracks hinder the further cracks propagation. Reasearch has suggested that crack toughening primarily improves inter granular strength at the micro level. Therefore, it is reasonable to conclude that the crack toughening phenomenon observed in alloy materials with a similar poly crystalline structure may also be applicable to some extent. However, crack toughening studies are mostly conducted from a two- dimensional perspective, and there may be differences in the selection of strength theories for alloy materials.

Based on the analysis of micro structural characterization and experimental curves, this study reasonably speculates that under the same loading conditions, a longer fatigue life correlates with a greater number of crack initiation sites. The presence of multiple initiation sites simultaneously inhibit specimen failure, thereby increasing the fatigue life. The entire failure process involves an interaction between the number of crack initiation sites and the number of cycles. However, this conclusion still lacks detailed experimental results and quantitative theoretical analysis for support. Further research and discussion are needed in future scientific work.

5. Conclusions

This paper combines experimental results, fracture surface characterization analysis, and finite element calculations to explain some experimental phenomena of different types of powder alloys under different mean stress conditions. The main research conclusions are as follows:

The cyclic life of the specimen under the condition of 650°C is not linearly related to the mean stress, but shows an "S"-shaped fluctuation trend with the increase of the mean stress, which is the result of a fatigue-creep coupling effect.

Failure mode analysis of fatigue fractures was carried out, and combined with creep-fatigue interaction theory, a reasonable explanation for the morphology characteristics of the number of crack initiation sites showing an "S"-shaped trend with the increase of mean stress was given: the lower the mean stress, the smaller the probability of crack initiation and the longer the cycle life of the material; With the increase of the mean stress, the probability of crack initiation increases, the number of crack sources increases, but at the same time, the decrease of stress amplitude reduces the crack propagation rate, leading to an increase in fatigue life. However, as the mean stress further increases, the crack initiation rate reaches a high level, causing the first crack source area to appear quickly, and then the crack expansion causes the specimen to fracture, resulting in a significant reduction in fatigue life.

The UCP constitutive model was used to simulate the specimen's cumulative damage and stress relaxation, and the analysis was performed in conjunction with the accumulated plastic strain obtained from experiments. The study revealed

that the damage during MAX-D primarily occurs in the first 2-3 cycles. Subsequently, due to rapid stress relaxation, the cumulative damage rate is almost zero in the subsequent cycles. However, throughout most cycles of the entire failure process, MIN-D exhibits higher Mises stress compared to MAX-D, regardless of whether it is at the peak or valley of loading. This leads to a steady accumulation of damage during the entire failure process under MIN-D conditions. These two factors collectively contribute to the gradual convergence of cumulative damage under both loading conditions, providing an explanation for the similarity in cycle counts between the two loading conditions.

By studying the micro structure and failure mechanism of the specimen fracture surface, combined with experimental data, the relationship between the number of crack initiation sites and the cycle life was analyzed and discussed. The conclusion is that under the same loading conditions, a larger cycle life will lead to more crack initiation sites, and multiple crack sources will inhibit specimen failure, thus increasing the cycle life. The entire failure process is the interaction between the number of crack initiation sites and the number of cycles.

Acknowledgement

This work was supported in part by the National Science and Technology Major Project under Grant J2019-IV-0011-0079 and J2019-IV-0003-0070; in part by the National Natural Science Foundation of China (Nos. 12302102)；in part by the Fundamental Research Funds of Shaanxi Key Laboratory of Artificially-Structured Functional Materials and Devices (AFMD-KFJJ-22204).

Conflict of Interest

There is no conflict of interest.

Supporting Information

Not applicable.

References

[1] C. Skamniotis, A.C.F. Cocks, Thermal and centrifugal stresses in curved double wall transpiration cooled components with temperature dependent thermoelastic properties, *International Journal of Solids and Structures*, 2022, **234-235**, 111273, doi: 10.1016/j.ijsolstr.2021.111273.

[2] C. Skamniotis, A.C.F. Cocks, Creep-plasticity-fatigue calculations in the design of porous double layers for new transpiration cooling systems, *International Journal of Fatigue*, 2021, **151**, 106304, doi: 10.1016/j.ijfatigue.2021.106304.

[3] G.C. Ngetich, A.V. Murray, P.T. Ireland, E. Romero, A three-dimensional conjugate approach for analyzing a double-walled effusion-cooled turbine blade, *Journal of Turbomachinery*, 2019, **141**, 011002, doi: 10.1115/1.4041379.

[4] H. Lu, J. Wang, Z. Wen, T. Liu, Y. Lian, Z. Yue, Vibration fatigue behavior and life prediction of directionally solidified superalloy based on the phase transformation theory, *Engineering Fracture Mechanics*, 2023, **282**, 109184, doi: 10.1016/j.engfracmech.2023.109184.

[5] J. Wang, H. Lu, Z. Wen, Y. Lian, Y. Wang, Z. Yue, Crystal plasticity theory coupled with meso-damage to predict the ratchetting behavior of nickel-based single crystal superalloy, *International Journal of Fatigue*, 2022, **165**, 107220, doi: 10.1016/j.ijfatigue.2022.107220.

[6] J. Wang, Y. Zhang, X. Wang, Z. Wen, Z. Yue, Thermodynamics-based method considering orientation and Notch effect to predict the high cycle fatigue life of a nickel-based single crystal superalloy, *International Journal of Fatigue*, 2023, **168**, 107452, doi: 10.1016/j.ijfatigue.2022.107452.

[7] C. Luo, H. Yuan, Life assessment of anisotropic low cycle fatigue of nickel-base single crystal superalloy, *International Journal of Fatigue*, 2023, **167**, 107310, doi: 10.1016/j.ijfatigue.2022.107310.

[8] V. Karamitros, D.W. MacLachlan, F.P.E. Dunne, Mechanistic fatigue in Ni-based superalloy single crystals: a study of crack paths and growth rates, *Journal of the Mechanics and Physics of Solids*, 2022, **158**, 104663, doi: 10.1016/j.jmps.2021.104663.

[9] C.M. Branco, J. Byrne, Fatigue behaviour of the nickel-based superalloy IN718 at elevated temperature, *Materials at High Temperatures*, 1994, **12**, 261-267, doi: 10.1080/09603409.1994.11752529.

[10] V. Brien, B. Décamps, Low cycle fatigue of a nickel-based superalloy at high temperature: deformation microstructures, *Materials Science and Engineering: A*, 2001, **316**, 18-31, doi: 10.1016/s0921-5093(01)01235-7.

[11] M. Bache, The effects of environment and loading waveform on fatigue crack growth in Inconel 718, *International Journal of Fatigue*, 1999, **21**, 69-77, doi: 10.1016/s0142-1123(99)00057-2.

[12] M.R. Bache, J. P. Jones, G. L. Drew, M. C. Hardy, N. Fox, Environment and time dependent effects on the fatigue response of an advanced nickel-based superalloy, *International Journal of Fatigue*, 2009, **31**, 1719-1723, doi: 10.1016/j.ijfatigue.2009.02.039.

[13] M.R. Bache, J. P. Jones, G. L. Drew, M. C. Hardy, N. Fox, Environment and time dependent effects on the fatigue response of an advanced nickel-based superalloy, *International Journal of Fatigue*, 2009, **31**, 1719-1723, doi: 10.1016/j.ijfatigue.2009.02.039.

[14] J. Telesman, T. P. Gabb, L. J. Ghosn, J. Gayda, Effect of notches on creep–fatigue behavior of a P/M nickel-based superalloy, *International Journal of Fatigue*, 2016, **87**, 311-325, doi: 10.1016/j.ijfatigue.2016.01.024.

[15] J. Zrnik, J. Semenak, P. Hornak, V. Vrchovinský, Lifetime behaviour of the wrought nickel base superalloy subjected to

low cycle fatigue with holds, *Kovove Materialy*, 2005, **43**, 93-104.
[16] L. Kunz, P. Lukáš, R. Konečná, High-cycle fatigue of Ni-base superalloy Inconel 713LC, *International Journal of Fatigue*, 2010, **32**, 908-913, doi: 10.1016/j.ijfatigue.2009.02.042.
[17] L. Kunz, P. Lukáš, R. Konečná, S. Fintová, Casting defects and high temperature fatigue life of IN 713LC superalloy, *International Journal of Fatigue*, 2012, **41**, 47-51, doi: 10.1016/j.ijfatigue.2011.12.002.
[18] G. Miao, X. Yang, D. Shi, Competing fatigue failure behaviors of Ni-based superalloy FGH96 at elevated temperature, *Materials Science and Engineering: A*, 2016, **668**, 66-72, doi: 10.1016/j.msea.2016.05.034.
[19] Z. Y. Lv, A. S. Wan, J. J. Xiong, K. Li, J. Z. Liu, Effects of stress ratio on temperature-dependent high-cycle fatigue properties of alloy steels, *International Journal of Minerals, Metallurgy and Materials*, 2016, **23**, 1387–96, doi: 10.1007/s12613-016-1362-5.
[20] L. Shui, Y. Xu, Z. Hu, Dislocation structure in a single crystal nickel base superalloy during high cycle fatigue at 870 ℃, *Rare Metal Materials and Engineering*, 2018, **47**, 1054-1058, doi: 10.1016/s1875-5372(18)30119-x.
[21] W. Cui, J. Wan, Z. Yue, Z. Yang, Tensile and low cycle fatigue properties of nickel-base powder metallurgy superalloy FGH95, *Rare Metal Materials and Engineering*, 2007, **36**, 2119-2123.
[22] X. Yang, L. Tan, T. Sui, D. Shi, Y. Fan, Low cycle fatigue behaviour of a single crystal Ni-based superalloy with a central hole: Effect of inhomogeneous rafting microstructure, *International Journal of Fatigue*, 2021, **153**, 106467, doi:10.1016/j.ijfatigue.2021.106467.
[23] Y. Xu, D. Hu, J. Mao, X. Liu, H. Sun, R.Wang. Powder superalloy short crack growth model considering effects of stress ratio and temperature, *Journal of Propulsion Technology*, 2023, **44**, 239-246, doi: 10.13675/j.cnki.tjjs.2207063.
[24] K. Tanaka, Y. Akiniwa, Y. Nakai, R. P. Wei, Modelling of small fatigue crack growth interacting with grain boundary, *Engineering Fracture Mechanics*, 1986, **24**, 803-819, doi: 10.1016/0013-7944(86)90266-3.
[25] H. W. Lee, C. Basaran, A review of damage, void evolution, and fatigue life prediction models, *Metals*, 2021, **11**, 609, doi: 10.3390/met11040609.
[26] C. Basaran, Introduction to Unified Mechanics Theory with Applications. Cham: Springer International Publishing, 2021, doi: 10.1007/978-3-030-57772-8.
[27] W. Egner, P. Sulich, S. Mroziński, H. Egner, Modelling thermo-mechanical cyclic behavior of P91 steel, *International Journal of Plasticity*, 2020, **135**, 102820, doi: 10.1016/j.ijplas.2020.102820.
[28] H. Wei Lee, H. Fakhri, R. Ranade, C. Basaran, H. Egner, A. Lipski, M. Piotrowski, S. Mroziński, Modeling fatigue of pre-corroded body-centered cubic metals with unified mechanics theory, *Materials & Design*, 2022, **224**, 111383, doi: 10.1016/j.matdes.2022.111383.
[29] N. Bin Jamal M, A. Kumar, C. Lakshmana Rao, C. Basaran, Low cycle fatigue life prediction using unified mechanics theory in Ti-6Al-4V alloys, *Entropy*, 2019, **22**, 24, doi: 10.3390/e22010024.
[30] H. W. Lee, C. Basaran, Predicting high cycle fatigue life with unified mechanics theory, *Mechanics of Materials*, 2022, **164**, 104116, doi: 10.1016/j.mechmat.2021.104116.
[31] H. W. Lee, C. Basaran, H. Egner, A. Lipski, M. Piotrowski, S. Mroziński, N. Bin Jamal M, C. Lakshmana Rao, Modeling ultrasonic vibration fatigue with unified mechanics theory, *International Journal of Solids and Structures*, 2022, **236-237**, 111313, doi: 10.1016/j.ijsolstr.2021.111313.
[32] M. Noushad Bin Jamal, L. R. Chebolu, C. Basaran, Unified mechanics theory based flow stress model for the rate-dependent behavior of bcc metals, *Materials Today Communications*, 2022, **31**, 103707, doi: 10.1016/j.mtcomm.2022.103707.
[33] H. W. Lee, M. B. Djukic, C. Basaran, Modeling fatigue life and hydrogen embrittlement of bcc steel with unified mechanics theory, *International Journal of Hydrogen Energy*, 2023, **48**, 20773-20803, doi: 10.1016/j.ijhydene.2023.02.110.
[34] M. R. Bache, J. O'Hanlon, D. J. Child, M. C. Hardy, High temperature fatigue behaviour in an advanced nickel based superalloy: the effects of oxidation and stress relaxation at notches, *Theoretical and Applied Fracture Mechanics*, 2016, **84**, 64-71, doi: 10.1016/j.tafmec.2016.03.007.
[35] P. J. Armstrong, C. O. Frederick, A mathematical representation of the multiaxial Bauschinger effect, Berkeley, CA: Berkeley Nuclear Laboratories, 1966, doi: 10.3184/096034007X207589.
[36] X. Lu, J. Zhao, C. Yu, Z. Li, Q. Kan, G. Kang, X. Zhang, Cyclic plasticity of an interstitial high-entropy alloy: experiments, crystal plasticity modeling, and simulations, *Journal of the Mechanics and Physics of Solids*, 2020, **142**, 103971, doi: 10.1016/j.jmps.2020.103971.
[37] A. Cruzado, J. LLorca, J. Segurado, Modeling cyclic deformation of inconel 718 superalloy by means of crystal plasticity and computational homogenization, *International Journal of Solids and Structures*, 2017, **122-123**, 148-161, doi: 10.1016/j.ijsolstr.2017.06.014.
[38] Z. Qi, B. Li, L. Xiong, An improved algorithm for McDowell's analytical model of residual stress, *Frontiers of Mechanical Engineering*, 2014, **9**, 150-155, doi: 10.1007/s11465-014-0295-9.
[39] X. Chen, R. Jiao, Modified mcdowell modeland ratcheting predictions of 1070 steel, *Engineering Mechanics*, 2005, **22**, 184-188.
[40] J. Hu, D. Li, B. Zhou, L. Cui, Z. Liu, Study on numerical simulation of W–Cu20 powder rolling based on Drucker-Prager/Cap model, *Powder Metallurgy Technology*, 2017, **35**, 249-254, doi: 10.19591/j.cnki.cn11-1974/tf.2017.04.002
[41] V. L. Berdichevsky, Overcoming paradoxes of Drucker–Prager theory for unconsolidated granular matter, *International Journal of Engineering Science*, 2014, **83**, 174-

186, doi: 10.1016/j.ijengsci.2014.03.004.
[42] C. Wang, L. Xiao, G. Zhang, J. Guo, A modified drucker-prager/cap model for powder metallurgy, *Rare Metal Materials and Engineering*, 2020, **49**, 3115-3121, doi: 10.12442/j.issn.1002-185X.2020.49.9.31153121.
[43] J. Wang, L. Yang, H. Lu, Z. Wen, T. Liu, Q. Yin, Z. Yue, Research on low cycle fatigue damage and macroscopic anisotropic constitutive model of Ni-based single crystal superalloy at different temperatures, *International Journal of Fatigue*, 2023, **177**, 107918, doi: 10.1016/j.ijfatigue.2023.107918.
[44] X. He, Y. Yao, An advanced constitutive model for SnPb and SnAg solder materials, 2014 15th International Conference on Electronic Packaging Technology. Chengdu, China. IEEE, 2014, 378-383, doi: 10.1109/ICEPT.2014.6922677.
[45] G. J. Rodin, Continuum damage mechanics and creep life analysis, *Journal of Applied Mechanics*, 2000, **67**, 193-196, doi: 10.1115/1.321163.
[46] X. Liu, C. Tao, D. Liu, Microscopic mechanism of fatigue damage for advanced nickel-base superalloys, *Rare Metal Materials and Engineering*, 2015, **44**, 3178-3182.
[47] G. Li, J. Guo, Z. Wang, H. Li, C. Shi, Effect of cyclic stress amplitude and mean stress on high temperature fatigue life of Ni_3Al (B) alloy, *International Journal of Fatigue*, 1996, **18**, 275, doi: 10.1016/0142-1123(96)89371-6.
[48] N. Bonora, A nonlinear CDM model for ductile failure, *Engineering Fracture Mechanics*, 1997, **58**, 11-28, doi: 10.1016/s0013-7944(97)00074-x.
[49] N. Bonora, G. M. Newaz, Low cycle fatigue life estimation for ductile metals using a nonlinear continuum damage mechanics model, *International Journal of Solids and Structures*, 1998, **35**, 1881-1894, doi: 10.1016/s0020-7683(97)00139-x.
[50] N. Bonora, On the effect of triaxial state of stress on ductility using nonlinear CDM model, *International Journal of Fracture*, 1997, **88**, 359-371, doi: 10.1023/A:1007479522972.
[51] Y. Huang, A user-material subroutine incroporating single crystal plasticity in the ABAQUS finite element program, Cambridge, UK: Harvard University, 1991.

